

Interaction of Spacecraft Arcjet Power Subsystem with Combined On orbit Environments and Electric Propulsion Plume: Ground Test Results

IEPC-2017-225

*Presented at the 35th International Electric Propulsion Conference
Georgia Institute of Technology • Atlanta, Georgia • USA
October 8 – 12, 2017*

Alexander L. Bogorad, Kevin August, Dr. Daniel Lichtin, John Pytel,
Kevin Payne, Dr. Roman Herschitz, Su Chad, Dr. Larry Capots, Barry Noakes, Ryan Dubisher
Lockheed Martin Space Systems, Littleton, CO, 80127, U.S.A.

Dr. Mitchell Walker
Georgia Institute of Technology, High-Power Electric Propulsion Lab, Atlanta, GA. 30332 U.S.A

Eugina D. Mendez Ramos
Georgia Institute of Technology, Aerospace Systems Design Lab, Atlanta, GA. 30332 U.S.A

Dr. Jonathan Walker and Nathaniel Prestridge
Georgia Institute of Technology, High-Power Electric Propulsion Lab, Atlanta, GA. 30332 U.S.A

Abstract: On-orbit observations and ground tests demonstrate the interaction between charged spacecraft and electrothermal thruster-generated plasma. On-orbit measurements and test results are presented for plasma diagnostics and solar array performance during long-term exposure of flight solar panels. The long-term performance of a several 70 V GEO solar array designs exposed to a 2 kW arcjet plasma environment as well as simulated 20-keV GEO electron plasma and solar flux was studied. Results confirm that interaction between plume and solar array strongly depended on space conditions, array design geometries, and surface coating configurations.

I. Nomenclature

<i>GEO</i>	=	Geostationary earth orbit
<i>NH₃</i>	=	Ammonia (gaseous)
<i>H₂</i>	=	Hydrogen (gaseous)
<i>I</i>	=	Current
<i>n_i</i>	=	Ion number density
<i>RGA</i>	=	Residual Gas Analyzer
<i>T_e</i>	=	Electron temperature
<i>V</i>	=	Voltage
<i>V_p</i>	=	Plasma potential

II. Introduction

Charging sensors [1], [2], [3] on several Lockheed Martin – manufactured geostationary earth orbit (GEO) spacecraft indicate that the presence of an ionized plasma plume due to the firing of electric propulsion thrusters (arcjets) will act to neutralize a charged spacecraft. As shown in Fig. 1, on-orbit data suggest, however, that charge dissipation is not immediate, and in fact, may take tens of seconds. The temporal delay results in the dense arcjet plume plasma being incident on a negatively-charged spacecraft / solar array system. The resulting condition is similar to those conditions shown to cause arcing in a Low Earth Orbit environment [4].

Arcjet thrusters are widely used for geosynchronous satellite station keeping. These thrusters have a proven flight history and have demonstrated high efficiency, high specific impulse, and high reliability within a wide range of electric power levels (0.2 – 2.2 kW). Temperatures of arcjet plume species, densities, and velocities have been measured inside the nozzle and in the near field up to 10 cm from the nozzle [5], [6], [7], and [8]. With typical geosynchronous (GEO) commercial satellite mission design lifetimes of 15 years or more a primary point of concern for designers and operators are the short and potentially long-term effects of the plume plasma on solar array operation. Common GEO commercial spacecraft solar arrays operate at voltages between 70 V and 100 V. The arcjet plume plasma density is sufficiently high to cause concern for increased current collection and associated power loss, ion-induced surface coating degradation, and electrostatic discharge propensity in a dense plasma. Although several studies of the plasma effects on solar arrays have been performed [9], [10], only limited long – term studies [11], [12] of the arcjet plume plasma effects have been published prior to the present study. Furthermore, none of the previous tests included combined environments such as high energy electrons and simulated solar and UV radiation. The current study simulates long-term effects of arcjet plume/space environment effects interaction with the solar array. Results confirmed that interaction between plume and solar array strongly depended on space conditions, array design geometries and surface coating configurations. Figure 1 shows typical changes in spacecraft potential as a result of arcjet firing.

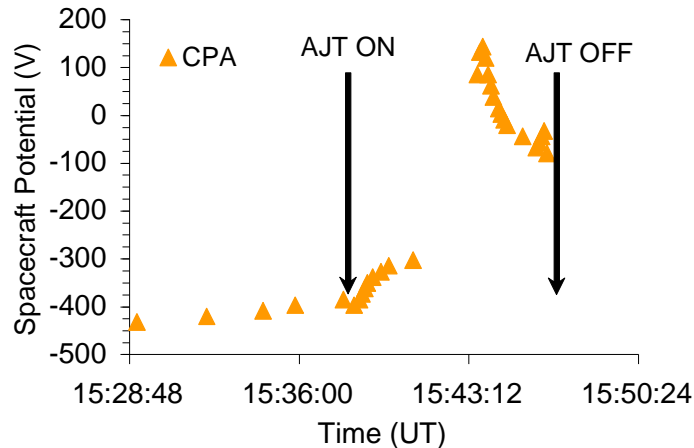


Figure 1. Geostationary spacecraft surface potentials as measured by Charge Potential Analyzer indicating response to arcjet firing.

III. Experimental Setup

A. Vacuum Chamber Facilities

Testing was performed at Georgia Institute of Technology, High-Power Electric Propulsion Laboratory. The vacuum chamber is 14 ft. in diameter by 22 ft. in length, and made of 316 stainless steel. The chamber utilizes six 48-in. diameter diffusion pumps, which allow the chamber to reach a base pressure of 10^{-7} Torr with a pump down time of two hours. The system is equipped to work with both flammable and toxic gases, which made this facility ideal for the solar array and arcjet testing.

B. Electrothermal Thruster and Solar Array

An Aerojet MR-510B arcjet thruster, shown in Figure 2, operating on simulated hydrazine, was mounted to the vacuum chamber floor with its nozzle mounted horizontally, as shown in Figure 2. The thruster was operated on a blend of certified ultra-high purity grade H_2 / N_2 (65% H_2 and 35% N_2) and ammonia (NH_3) to simulate the decomposition of hydrazine (N_2H_4) at typical arcjet flow rates given by



The GEO flight solar array panels were mounted down bore site of the arcjet as shown in Figure 3. Solar array 1 consisted 3 Advanced Triple-Junction (ATJM) solar cells strings and 2 Ultra Triple-Junction (UTJ) strings wired and laid on a composite substrate with aluminum honeycomb core.

Solar array 2 consisted of larger third generation triple-junction (ZTJ) cells mounted on the flexible substrate. Solar array 3 consisted of the ZTJ cells mounted on a rigid substrate. The strings on each panel were laid out to simulate a typical GEO solar panel configuration and flight representative inter-cell spacing and numbers of repaired interconnects. As is the common GEO design convention, the solar cells include an anti-reflective coating and a charge dissipative coating. All materials and processes used to build the panels were per qualified flight processes, designs, and materials.

To accurately simulate the worst-case GEO spacecraft charging condition, the entire solar panel was exposed to a 20 keV high-energy electron beam using a Kimball Physics flood gun (EGF-3104). Furthermore, the solar array was illuminated to ~ 0.5 suns and was generating power throughout the test utilizing a custom-build ScienceTech Inc. solar simulator with an unfiltered 5-kW xenon lamp. The solar arrays were radiative cooled by a cold plate to stay within observed on-orbit operating temperatures. The solar array and arcjet system were electrically isolated from the chamber (earth) ground.

C. Diagnostics

The set of diagnostics tools used included three spherical Langmuir probes (LPs), one emissive probe (EP), a Residual Gas Analyzer (RGA), and an emission spectrometer. The emissive and Langmuir probes were constructed using the Air Force Research Lab standard [13] and were mounted along the periphery of the solar array cooling plate and support stand as shown in Figure 4. The perpendicular distance between the probe and array was approximately 5 inches. The RGA (Stanford Research Systems, RGA200) is located on the ceiling of the vacuum chamber, between the solar array and the arcjet, and was placed 12.6 in. downstream of the arcjet nozzle and 63.7 in. from the arcjet centerline. The emission spectrometer (Ocean Optics, HR4000CG-UV-NIR) was located directly opposite the solar array, perpendicular to the arcjet centerline, at the chamber wall. Diagnostic equipment also included multiple video cameras.

The solar panel was wired such that each string could be biased independently of other strings allowing for optimal flexibility in current collection and breakdown voltage measurements. Each string and the panel substrate were continuously monitored for bias voltage and current, string voltage and current, and temperature via three spatially isolated thermocouples between the cold plate and solar array substrate. Plasma collection current of the exposed strings was obtained by shorting the positive and return of the string and measuring the current at each of the biased voltages without the solar simulator. Solar array string diagnostics consisted of a limited light IV and Dark IV. Light IV measured three critical points; shunted/shorted current, current at 70 V across the string, and open circuit voltage. The measurement is useful for determining the health of the coverglass. Dark IV used a Keithly 2410 to step the voltage across the string. This measurement is useful for determining the semiconductor health, P-N junction shorting, and bypass diode health.

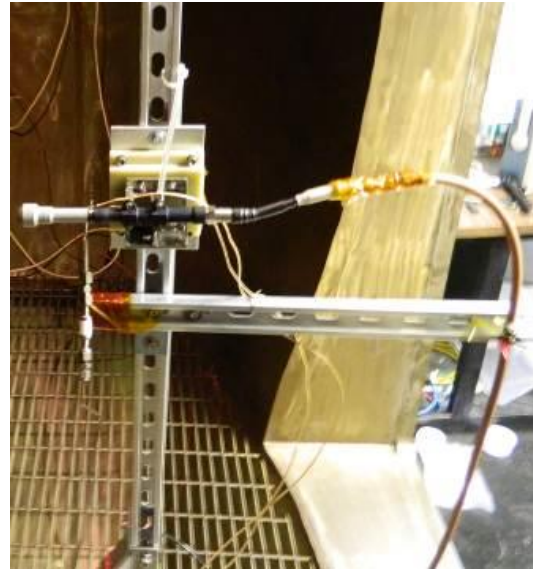


Figure 2. MR-510B arcjet and stanchion as configured for test.



Figure 3. Solar panel and panel-mounted diagnostics equipment as suspended in test chamber.

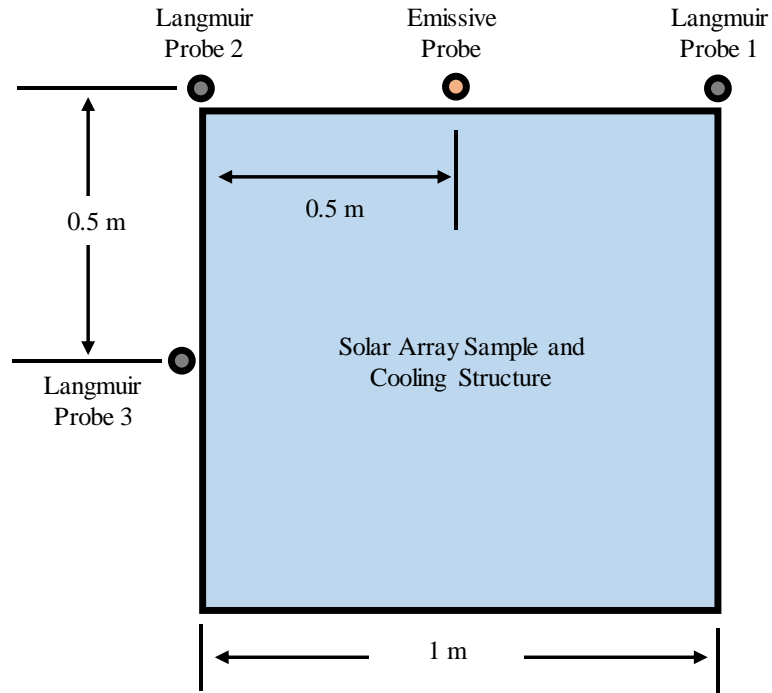


Figure 4. Emissive and Langmuir probe locations.

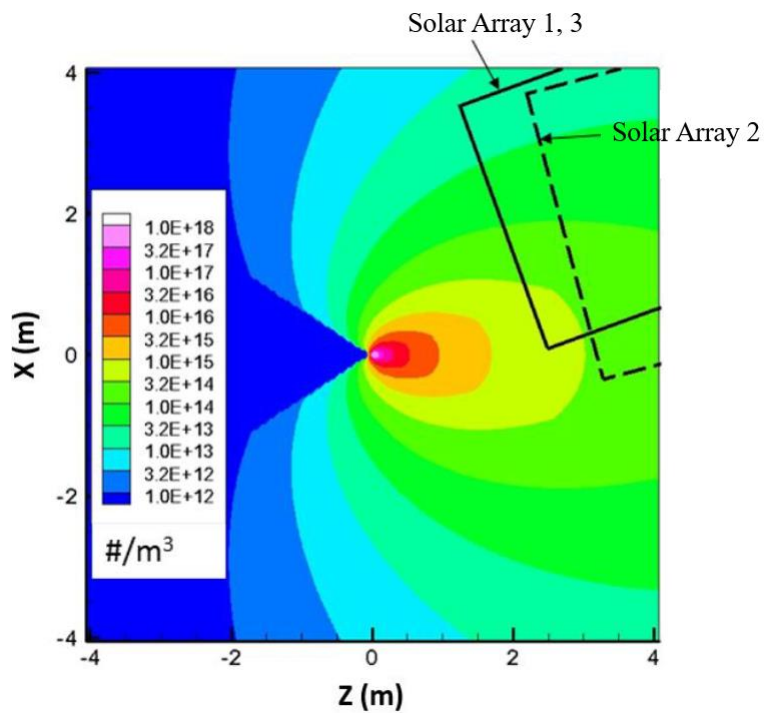


Figure 5. Plasma density at lower panel position¹².

IV. Experimental Test and Methods

A. Short-Term Solar Array Evaluation

A short-term test was run to determine solar array performance during spacecraft charging events. String bias voltages were set between 0 and -250 V using power supplies and control equipment outside of the chamber. The arcjet was started in two configurations to determine the effects of bias on the solar array cells, interconnects, and coverglass. To monitor for visual electrical effects, two sets of experimental configurations were performed, alternating every arcjet run.

1. Biased without Solar Simulator

The solar simulator was not operating. The positive and the return of the strings were shorted together and biased to the desired voltage. Collection currents were recorded during these conditions. After a short time, the solar simulator was started, and the bias voltage on the return was set to the arcjet cathode and the strings were set to 70 V positive to the return.

2. Biased with Solar Simulator

During the other half of the biased runs, the solar simulator was on and the solar array was set to 70 V with the return biased to the desired bias voltage. The arcjet was started and the bias was removed and then set to arcjet cathode floating bias (~1V) after a few minutes. Light IV and Dark IV solar array diagnostics were performed after every arcjet run. Two different cameras attempted to capture visual effects of biased solar arrays in the plasma.

B. Long-Term Solar Array Evaluation

The unbiased long-term effects on the solar array were performed for 300 hours. This sequence started with the solar array return set to arcjet cathode floating bias (~1 V) and the solar simulator continuously operating. To assess solar array performance, Light IV measurements were performed after every 1-hour run and Dark IV measurements were performed approximately every four runs.

C. Plasma Plume Characterization

Figure 5 shows detailed plume maps generated analytically based on published exit plane and near field measurements [14]. The plume maps are consistent with earlier measurements. [12]. The plasma density of the arcjet plume near the solar array is estimated to be on the order of 10^{14} particles/m³ and the Debye length of the plasma is estimated to be on the order of 1 mm. Typical spatial distribution of plasma density was consistent with earlier measurements and is shown in Figure 6 and described by the fitting equation

$$n(z) = 3.185 \times 10^{14} z^{-1.29} m^{-3} \quad (2)$$

where z denotes the distance from the nozzle (cm). Fitting data using Equation (2) at near field distances yield results which are in agreement with previously published measurements [6], [15]. It can be concluded that the plasma expands with nearly constant velocity as the density is shown to decrease in near accordance to the inverse square law.

The properties of the quasi-neutral plasma surrounding the solar array sample were determined from analysis of the data collected from the emissive and Langmuir probes. Current-voltage (I-V) sweeps were collected for the following test conditions: (1) closed, empty chamber, (2) with solar array in place, and (3) with the solar array biased. Plasma potentials were determined from analysis of the emissive probe data via the techniques developed by [20] and

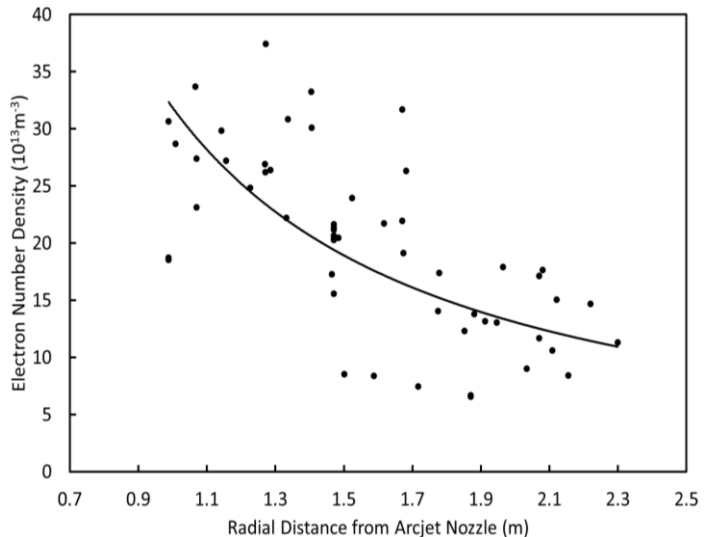


Figure 6. Electron number density as a function of radial distance from the arcjet nozzle. The electron number density varies according to inverse square law.

[21]. Standard data interpretation techniques for plasma sheath theory applied to spherical Langmuir probes were used to calculate the electron temperature and ion number densities probe data.

V. Results

The results confirm findings of previous studies [1], [2], [10], [12], [17] that show biased spacecraft surfaces (especially negatively-biased metallic components) interact with the plasma plume. The interactions can cause arcing and glow discharges that under extreme conditions can cause damage to some types of solar cells. Figure 7 shows the glow from one of the solar arrays during the exposure test. Figure 8 is a simple rendering of Figure 7, and provides scale and the location of the glow with respect to the array. The floating potential of common arcjet/solar array return was measured to be ~ 1 V relative to chamber ground. In addition, the results shows that the current collected by the solar panel is not sufficient to impact power subsystem performance (<1 % loaded string current loss).

A. Short-Term (Biased) Exposure

The multi-level biased exposures of the arrays demonstrated that the exposed, biased, components of the solar array are highly susceptible to damaging electrical interactions with the arcjet plasma. Glow discharges and primary arcing eventually damages the cell, reducing the power output of the string. Eventually, if the spacecraft becomes biased to low enough negative voltages during arcjet firings, enough cells are removed from the string to drop off the bus.

B. Long-Term (Unbiased) Exposure

Solar panels that showed immunity to short term arcing effects, are subjected to 300 arcjet starts and to continuous arcjet plume exposure of approximately 300 hours to evaluate effects of long-term exposure to the arcjet plume. Long – term exposure results indicate:

1. No changes in coverglass coating continuity or string isolation
2. No degradation of cell
3. No changes in solar array power output

C. Plasma Plume Characterization

The analysis theory discussed previously for the emissive and Langmuir probes is used to calculate the plasma parameters. The plasma parameters obtained for the three solar arrays are reported in 0 and Appendix B:. Note that the Langmuir probes were installed August 2016, while installation of the single emissive probe was completed in October 2016. Due to the nature of the experiment, there were instances where data collection was interrupted by a failed arcjet fire or other related experimental interruption. While corresponding data from both emissive and Langmuir probes was the goal, it was not always possible. Although plasma potential can be determined from I-V curve analysis of data collected from a Langmuir probe, the emissive probe provides better estimates of plasma potential and less overall error. Thus, only plasma potentials measured with the emissive probe are presented in this manuscript.

The measured plasma potentials are listed in Table A. 1 and Table A. 2. A set three $\ln(I)$ -V curves are collected at each condition. The average of the three calculated plasma potentials is presented. For the unbiased test condition, the plasma potential ranges from 1.63 V to 5.09 V ± 2 V. For cases where a bias was applied to the solar array, the average plasma potential ranges from 0.02 V to 4.19 V ± 2 V.

The values for the electron temperature and ion number density obtained from analysis of the Langmuir probe are presented in Appendix B:. A set of five $\ln(I)$ -V curves are collected at each condition. The average of five calculated electron temperatures is presented. The electron temperature ranges from 1.31 eV to 4.41 eV ± 0.5 in the unbiased test case, and ranges from 0.22 to 4.45 eV ± 0.5 for the biased case. The ion number densities ranges from 2.2×10^{12} #/m³ to 3.5×10^{14} #/m³ for the unbiased case, and ranges from 9.1×10^{11} #/m³ to 1.9×10^{14} #/m³ for the biased case.



Figure 8. Glow discharges on solar array sample.

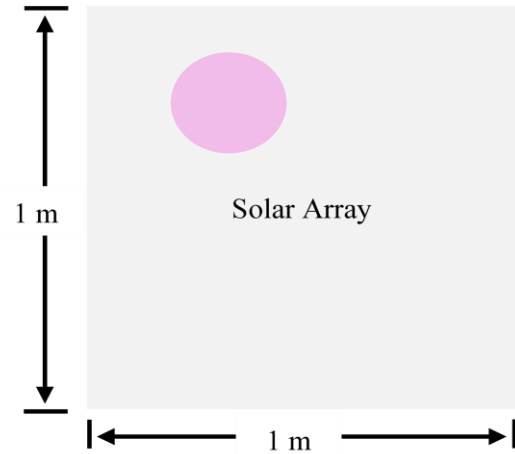


Figure 7. Dimensions of solar array and location of glow discharge.

D. Residual Gas Analyzer and Emission Spectrometer

The RGA was used as an additional diagnostic during testing to detect the presence of tungsten, in the event of throat deterioration in the arcjet, and other contaminants. It should be noted that the chamber pressure was too high during arcjet firing for the RGA filament to run without damage. Scans were taken shortly after the arcjet ceased firing. A typical scan is displayed in Figure C. 1, located in Appendix C:. If tungsten were present in the chamber environment, a distinct peak would be expected at 183 amu, and as can be seen from the figure, no discernable peak is present. If tungsten was indeed present, the amount was below the detection sensitivity of the RGA. The substances detected (by percent mass) in the scan are listed in Table C. 1. Again, notice that tungsten is not listed as one of the molecular species identified to be present in a quantity greater than the sensitivity of the RGA.

An emission spectrometer used in the arcjet solar array testing was configured for maximum range and maximum resolution, imparting lower sensitivities to the instrument. Hence, the data did not show any significant peaks above the noise threshold.

VI. Discussion

The study aims to characterize the response of a solar array exposed to the arcjet plasma plume as a function of electrical configuration. To have a known plasma exposure, the exhaust plume was interrogated in intervals during hundreds of hours of thruster operation. As the thruster components erode with time, the plasma characteristics evolve. The discussion validates the plasma measurements in the arcjet exhaust as a function of arcjet operating time.

Figure 4 shows the locations of the emissive probe with respect to the solar array structure. The plasma sheath calculated from the measured electron number density and electron temperature ranges from 0.5 cm to 8.8 cm. Thus, there is no interaction between the plasma probes and the electrical biasing of the solar arrays. This prediction is supported by the absence of correlation between the measured plasma potential and the solar array electrical configuration. Any variation present in the plasma measurements is due to uncertainties in the geometry of the probes, measurements of current and voltage, probe analysis techniques, and variation in the facility pressures.

The arcjet plume is unique because it is composed of multiple ionic species that result from propellant composed of N_2 , H_2 , and NH_3 . Hence, the ions in the plume population may be composed of different species and physical processes that are not accounted for in the probe theory used to determine the plasma potential. It is assumed that all species fractions are in steady state. However, it would be interesting to identify the ion fractions for each species to gain further understanding of their effect on the interpretation of the I-V analysis.

Long-term tests confirmed that arcjet plume has limited interaction with the solar array under normal conditions. Following such exposure, no array degradation of performance or any in-situ ESD events were detectable. Collected array currents were small and caused minimal power decrease (<1%). On the other hand, arcjet firing during spacecraft charging events, when the spacecraft is charged negatively by GEO plasma, can result in significant interaction between the arcjet plume and the solar array. These interactions can damage the solar array cells and surface coatings. The severity of the interaction is highly dependent on local geometries. In addition, thin insulating films are

susceptible to electrically breakdowns that damage such films. For plasma conditions present during charging events, many design practices recommended for low orbits in NASA_HDBK_4006 provide useful guidance.

VII. Conclusion

On-orbit observations confirm the existence of the interaction between spacecraft and electrothermal thruster-generated plasma plume. A high-fidelity ground test of a flight – like arcjet and solar array – has produced valuable results to further the understanding of the long term and complex effects of plume spacecraft interactions. Far field (>2 m) arcjet plume diagnostics were performed in a voluminous vacuum chamber and have yielded results that can be extrapolated favorably to publish near field data. Results of ground testing and analyses presented here confirm that during NSSK maneuvers GEO solar arrays are exposed to a plasma density similar to that of LEO. Test results indicate no significant long-term degradation of the solar array or cell coatings and no evidence of surface contamination under normal operating conditions. However, the long-term effects arcjet plume combined with GEO plasma on solar array operation should be considered by spacecraft designers and operators. Results of the current study confirmed that interaction between plume and solar array strongly depended on space conditions, array design geometries, and surface coating configurations.

Current collected by solar array from plasma plume results in a <1% power loss during arcjet firing, which is not sufficiently high to impact system performance. Current collection effects and possible plasma-induced electrical breakdown should be considered by solar array system and spacecraft designers seeking to develop design strategies for an ESD hardened, higher reliability solar array. Additional hardening measures that have demonstrated success in orbit on GEO solar arrays include the use prudent string layouts which maximize spacing between adjacent strings and circuits, reduced voltage gradients between strings/circuits and the use of RTV silicone grouting between solar cells. String layouts should limit a maximum voltage difference between adjacent strings/circuits during steady state operation and also during periods of circuit shunting. String layouts should also seek to ensure the maximum achievable inter-cell spacing. Finally, avoiding geometries and coatings configurations that can result in high electric fields will significantly limit the interaction.

Appendix A: Plasma Potential

Table A. 1. Solar Array 2

*Date (MM/DD/YYYY)	Bias (V)	Plasma Potential (V)
10/12/2016	-185	2.6
10/12/2016	-205	4.2
10/12/2016	-215	0.7
10/12/2016	-215	0.0
10/31/2016	0	4.0
11/1/2016	0	2.2
11/4/2016	0	2.6
11/7/2016	0	2.4
11/8/2016	0	2.3
2/14/2017	0	1.6
2/15/2017	0	1.8
2/27/2017	0	5.1

Table A. 2. Solar Array 3

*Date (MM/DD/YYYY)	Bias (V)	Plasma Potential (V)
5/12/2017	-150	2.7
5/13/2017	-250	2.5
5/17/2017	-70	2.2

* Test pressures ranges: 10^{-4} Torr to 10^{-6} Torr

Appendix B: Electron Temperature and Ion Number Density

Table B. 1. Solar Array 1

*Date (MM/DD/YYYY)	Probe Position	Bias (V)	Electron Temperature (eV)	Ion Number Density (#/m³)
8/8/2016	L1	-70	0.4	7.3 x 10 ¹²
8/8/2016	L2	-70	0.3	1.0 x 10 ¹⁴
8/8/2016	L1	-70	0.6	3.0 x 10 ¹³
8/8/2016	L2	-70	0.3	4.7 x 10 ¹³
8/8/2016	L3	-70	0.6	7.4 x 10 ¹³
8/8/2016	L2	-70	0.4	4.0 x 10 ¹³
8/9/2016	L1	-100	0.4	2.5 x 10 ¹³
8/9/2016	L2	-100	0.5	2.7 x 10 ¹³
8/9/2016	L3	-100	0.2	1.2 x 10 ¹⁴
8/9/2016	L1	-100	0.5	2.2 x 10 ¹³
8/9/2016	L2	-100	0.5	2.4 x 10 ¹³
8/9/2016	L3	-100	0.2	1.2 x 10 ¹⁴
8/9/2016	L1	-100	0.4	2.4 x 10 ¹³
8/9/2016	L2	-100	0.5	2.6 x 10 ¹³
8/9/2016	L3	-100	0.2	1.1 x 10 ¹⁴
8/9/2016	L1	-100	0.4	2.3 x 10 ¹³
8/9/2016	L2	-100	0.5	2.7 x 10 ¹³
8/9/2016	L3	-100	0.2	1.1 x 10 ¹⁴
8/9/2016	L1	-100	0.7	1.2 x 10 ¹³
8/9/2016	L3	-100	0.5	5.8 x 10 ¹³
8/15/2016	L1	-250	1.3	9.1 x 10 ¹¹
8/15/2016	L2	-250	1.3	1.4 x 10 ¹³
8/15/2016	L3	-250	1.1	8.0 x 10 ¹²
8/23/2016	L1	0	1.6	2.2 x 10 ¹²
8/23/2016	L2	0	1.4	3.4 x 10 ¹²
8/23/2016	L3	0	1.3	7.0 x 10 ¹²
5/2/2017	L1	-100	4.4	6.6 x 10 ¹³
5/2/2017	L2	-100	4.5	1.1 x 10 ¹⁴
5/2/2017	L3	-100	4.3	1.9 x 10 ¹⁴
5/4/2017	L1	-150	4.3	7.1 x 10 ¹³
5/4/2017	L2	-150	4.4	1.2 x 10 ¹⁴
5/4/2017	L3	-150	4.3	1.8 x 10 ¹⁴
5/6/2017	L1	-150	4.3	7.1 x 10 ¹³
5/6/2017	L2	-150	4.4	1.2 x 10 ¹⁴
5/6/2017	L3	-150	4.3	1.8 x 10 ¹⁴

* Test pressures ranges: 10⁻⁴ Torr to 10⁻⁶ Torr

Table B. 2. Solar Array 2

*Date (MM/DD/YYYY)	Probe Position	Bias (V)	Electron Temperature (eV)	Ion Number Density (#/m³)
10/9/2016	L1	-70	2.2	2.6 x 10 ¹³
10/9/2016	L2	-70	2.2	4.9 x 10 ¹³
10/9/2016	L3	-70	1.9	8.2 x 10 ¹³
10/9/2016	L1	-70	2.0	4.6 x 10 ¹³
10/9/2016	L3	-70	1.8	1.0 x 10 ¹⁴
10/11/2016	L1	0	1.8	3.5 x 10 ¹³
10/11/2016	L2	0	2.0	7.7 x 10 ¹³
10/11/2016	L3	0	1.8	1.3 x 10 ¹⁴
10/11/2016	L1	-175	1.8	4.1 x 10 ¹³
10/11/2016	L2	-175	2.1	7.7 x 10 ¹³
10/31/2016	L1	0	2.7	9.7 x 10 ¹²
10/31/2016	L2	0	3.4	1.9 x 10 ¹³
10/31/2016	L3	0	3.0	3.4 x 10 ¹³
11/1/2016	L1	0	2.7	9.0 x 10 ¹²
11/1/2016	L2	0	3.1	1.8 x 10 ¹³
11/1/2016	L3	0	2.8	2.5 x 10 ¹³
11/4/2016	L1	0	2.7	1.1 x 10 ¹³
11/4/2016	L2	0	3.0	2.1 x 10 ¹³
11/4/2016	L3	0	2.8	2.8 x 10 ¹³
11/7/2016	L1	0	2.6	1.1 x 10 ¹³
11/7/2016	L2	0	2.9	2.2 x 10 ¹³
11/7/2016	L3	0	2.7	2.8 x 10 ¹³
11/8/2016	L1	0	2.5	1.2 x 10 ¹³
11/8/2016	L2	0	2.9	2.2 x 10 ¹³
11/8/2016	L3	0	2.7	3.4 x 10 ¹³
2/14/2017	L1	0	3.7	4.5 x 10 ¹³
2/14/2017	L2	0	3.9	9.8 x 10 ¹³
2/14/2017	L3	0	3.5	1.9 x 10 ¹⁴
2/15/2017	L1	0	3.5	5.5 x 10 ¹³
2/15/2017	L2	0	3.9	1.2 x 10 ¹⁴
2/15/2017	L3	0	3.3	2.1 x 10 ¹⁴
2/27/2017	L1	0	3.6	5.0 x 10 ¹³
2/27/2017	L2	0	3.9	1.1 x 10 ¹⁴
2/27/2017	L3	0	3.6	2.1 x 10 ¹⁴

* Test pressures ranges: 10⁻⁴ Torr to 10⁻⁶ Torr

*Date (MM/DD/YYYY)	Probe Position	Bias (V)	Electron Temperature (eV)	Ion Number Density (#/m³)
3/7/2017	L1	0	3.7	6.9 x 10 ¹³
3/7/2017	L2	0	4.4	1.5 x 10 ¹⁴
3/7/2017	L3	0	4.1	2.8 x 10 ¹⁴
3/8/2017	L1	0	3.8	7.3 x 10 ¹³
3/8/2017	L2	0	4.3	1.6 x 10 ¹⁴
3/8/2017	L3	0	3.9	2.9 x 10 ¹⁴
3/9/2017	L1	0	4.1	7.5 x 10 ¹³
3/9/2017	L2	0	4.2	1.6 x 10 ¹⁴
3/9/2017	L3	0	3.9	2.9 x 10 ¹⁴
3/16/2017	L1	0	4.4	8.5 x 10 ¹³
3/16/2017	L2	0	4.4	2.1 x 10 ¹⁴
3/16/2017	L3	0	4.2	3.5 x 10 ¹⁴
4/8/2017	L1	0	4.1	6.7 x 10 ¹³
4/8/2017	L2	0	4.3	1.3 x 10 ¹⁴
4/8/2017	L3	0	4.0	2.4 x 10 ¹⁴
4/10/2017	L1	0	4.2	8.0 x 10 ¹³
4/10/2017	L2	0	4.3	1.6 x 10 ¹⁴
4/10/2017	L3	0	3.9	2.2 x 10 ¹⁴
3/7/2017	L1	0	3.7	6.9 x 10 ¹³
3/7/2017	L2	0	4.4	1.5 x 10 ¹⁴
3/7/2017	L3	0	4.1	2.8 x 10 ¹⁴

* Test pressures ranges: 10⁻⁴ Torr to 10⁻⁶ Torr

Appendix C: Residual Gas Analyzer

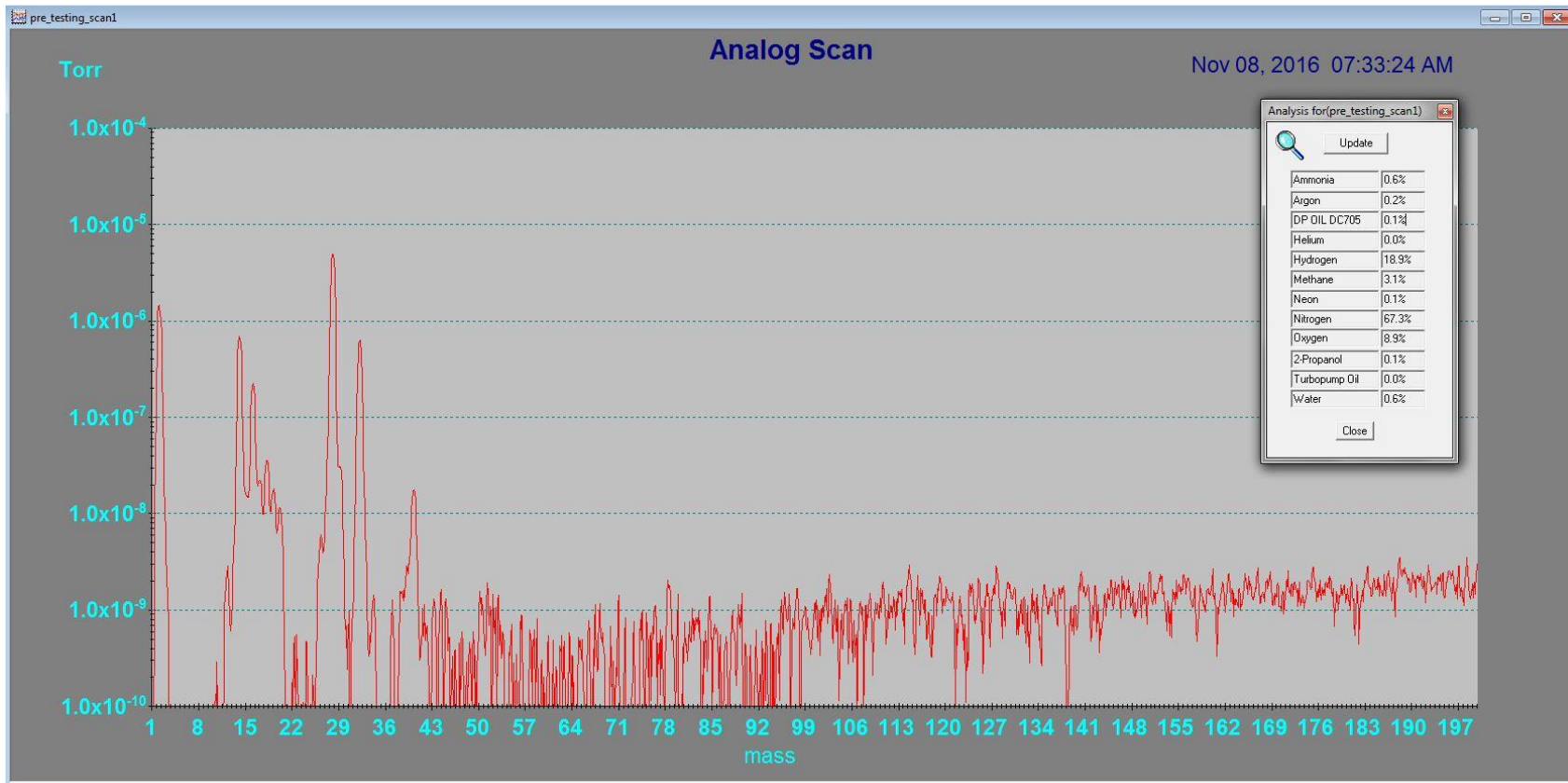


Figure C. 1. Representative RGA scan

Table C. 1. Substances detected by RGA

Molecule/Substance	Percentage Detected
Ammonia	0.6%
Argon	0.2%
DP Oil 705DC	0.1%
Helium	0.0%
Hydrogen	18.9%
Methane	3.1%
Neon	0.1%
Nitrogen	67.3%
Oxygen	8.9%
2-Propanol	0.1%
Turbo pump oil	0.0%
Water	0.6%

Acknowledgements

The authors are grateful for the services, support and the considerable efforts of C. R. Roberts of RNR Engineering in the design, analysis, and operation of the on – site arcjet propulsion and electrical systems and D. Zube at Aerojet for technical consultations.

References

- [1] Ozkul, A., Lopatin, A., Shipp, A., Pitchford, D., Mazur, J., Roeder, J., Koons, H., Bogorad, A., and Herschitz, R. "Initial Correlation Results of Charge Sensor Data from Intelsat VIII Class Satellites with Other Space and Ground Measurements." *Proceedings of the 7th Spacecraft Charging Technology Conference*, ESA Pub. Div. SP-476, Noordwijk, the Netherlands. Nov. 2001.
- [2] Koons, H., Mazur, J., Lopatin, A., Pitchford, D., Bogorad, A., and Herschitz, R. "Spatial and Temporal Correlation of Spacecraft Surface Charging in Geosynchronous Orbit," *J. Spacecraft and Rockets*, Vol. 43, No. 1, January-February 2006, pp. 178-185.
- [3] Bogorad, A., Bowman, C., Dennis, A., Beck, J., Lang, D., Herschitz, R., Buehler, M., Blaes, B., and Martin, D. "Integrated Environmental Monitoring System for Spacecraft," *IEEE Trans. Nuc. Sci.*, Vol. 42, No. 6, December 1995 pp. 2051-2057.
- [4] Ferguson, D. and Hillard, G. B. "Low Earth Orbit Spacecraft Charging Design Guidelines," NASA / TP – 2003 – 212287, February 2003.
- [5] Zube, D.M. and Myers, R.M. "Thermal Nonequilibrium in a Low Power Arcjet Nozzle," *J. Propulsion and Power*, Vol. 9, No. 4, 1993, pp. 545 – 552.
- [6] Zube, D.M., Fye, D., Masuda, I., Gotoh, Y. "Low Bus Voltage Hydrazine Arcjet System for Geostationary Satellites," *Proceedings of 34th AIAA Joint Propulsion Conference*, July 13-15, 1998, Cleveland, OH, USA (AIAA Paper 98-3631).
- [7] Crofton, M.W., Moore, T.A., Boyd, I.D., Masuda, I., and Gotoh, Y. "Near-Field Measurement and Modeling Results for Flight – Type Arcjet: Hydrogen Atom," *J. of Spacecraft and Rockets*, Vol. 38, No. 3, 2001, pp. 417 – 425.
- [8] Pollard, J.E., Masuda, I., and Gotoh, Y. "Plume Mass Spectrometry with Hydrazine Arcjet Thruster," *J. of Spacecraft and Rockets*, Vol. 38, No. 3, 2001, pp. 411 – 416.
- [9] Meulenbergh, A. "Overview, Testing, and Solutions to ESD – Induced Solar Array String, On-orbit Failures," *Progress in Photovoltaics Research and Applications*, Vol. 8, 2000, pp. 315 – 321.
- [10] Leung, P. "Plasma Phenomena Associated with Solar Array Discharges and Their Role in Scaling Coupon Test Results to a Full Panel," *Proceedings of 40th Aerospace Sciences Meeting and Exhibit*, January 14 – 17, 2002, Reno, NV, USA, Paper 2002 – 0628.
- [11] Bogorad, A., Lichtin, D., Bowman, C., Armenti, J., Pencil, E., and Sarmiento, C. "The Effects of 1kW Class Arcjet Thruster Plumes on Spacecraft Charging and Spacecraft Thermal Control Materials," *IEEE Trans. Nuc. Sci.*, Vol. 39, No. 6, December 1992, pp. 1783 – 1789.
- [12] Justin Likar, Alexander Bogorad, Thomas Malko, Neil Goodzeit, Joel Galofaro, Myron Mandel, "Interaction of Charged Spacecraft with Electric Propulsion Plume: On Orbit Data and Ground Test results" *IEEE Trans. Nuc. Sci.*, Vol. 53, No. 6, December 2006.
- [13] Xu, Kunning Gabriel. *Ion collimation and in-channel potential shaping using in-channel electrodes for Hall effect thrusters*. Georgia Institute of Technology, 2012.
- [14] Mandell, M.J., Davis, V.A., Kuharski, R.A., and Jongeward, G.A. "SAIC Calculations in Support of Lockheed Martin Solar Array Ground Testing," Unpublished report, December 2004.
- [15] Galofaro, J., Vayner, B., Hillard, G. and Chornak, M. "Thruster Plume Plasma Diagnostics: A Ground Chamber Experiment for a 2-Kilowatt Arcjet", NASA TM-2005-213837, July 2005, *Prepared for the 6th Frontiers in Low-Temperature Plasma Diagnostics Workshop*, Laboratoire de Spectrometrie Physique, Les Houches, France, April 17-21, 2005.
- [16] Ling, H., Kim, H., Hallock, G., Brickner, G., and Zaman, A. "Effect of Arcjet Plume on Satellite Reflector Performance," *IEEE Transactions on Antennas and Propagation*, Vol. 39, No. 9, September 1991, p. 1412 – 1420.
- [17] Vayner, B., Galofaro, J., and Ferguson, D. "Interactions of High Voltage Solar Arrays with Their Plasma Environment: Physical Processes," *Journal of Spacecraft and Rockets*, Vol. 41, No. 6, 2004, p. 1031 – 1041.
- [18] Sato, T., Takahashi, M., Nakamura, M., Kawakita, S., Cho, M., Toyoda, K., and Nozaki, Y. "Development of Solar Array for a Wideband Internetworking Engineering Test and Demonstrating Satellite: System Design," *Proceedings of the 8th Spacecraft Charging Technology Conference*, October 20-24, 2004, Huntsville, AL, USA.
- [19] Ferguson, D. and Hillard, G. B. "Low Earth Orbit Spacecraft Charging Design Guidelines," NASA / TP – 2003 – 212287, February 2003.
- [20] Demidov, V. I., R. S. V. and Rypdal, K., "Electric probes for plasmas: The link between theory and instrument," *Review of Scientific Instruments*, Vol. 73, 2002, pp. 3409–3439.
- [21] Sheehan, J. P. and Hershkowitz, N., "Emissive probes," *Plasma Sources Science & Technology*, Vol. 20, No. 6, 2011.